ELSEVIER

International Journal of Solids and Structures 41 (2004) 435–457

INTERNATIONAL JOURNAL OF SOLIDS and STRUCTURES

www.elsevier.com/locate/ijsolstr

Computational multiple scattering analysis for shear wave propagation in unidirectional composites

S. Biwa *, S. Yamamoto, F. Kobayashi, N. Ohno

Department of Micro System Engineering, Nagoya University, Furo-cho, Chikusa-ku, Nagoya 464-8603, Japan

Received 3 March 2003; received in revised form 16 July 2003

Abstract

A computational procedure for multiple wave scattering in unidirectional fiber-reinforced composite materials is presented. The present study deals with the time-harmonic propagation of shear waves polarized parallel to the fibers. The exciting and scattered fields for each fiber are expressed by the eigenfunction expansion, and a collocation method is used to determine the expansion coefficients numerically. With this procedure, detailed aspects of the shear wave scattering and propagation in unidirectional SiC/Ti-alloy composite with periodic as well as random fiber arrangements are demonstrated, including the dispersion relation and the energy transmission behavior. The analysis recovers that the wave with a sufficiently long wavelength propagates as a sinusoidal plane wave insensitively to the fiber arrangement. As the wavelength becomes comparable to the fiber spacing, the wave field gains complicated appearances specific to the fiber arrangement. For the periodic fiber arrangements, it is shown that the wave ceases to propagate in the composite in certain frequency bands. The wave fields in such stop bands are shown to possess a standing-wave nature and involve spatially decaying amplitudes and vanishing energy flow in the propagation direction. Numerical results are also shown for a random fiber distribution in order to demonstrate the applicability of the present scheme to arbitrary fiber arrangements. The computed phase velocities and the energy transmission ratios for the random composite compare favorably with those predicted by an existing multiple scattering theory.

Keywords: Fiber-reinforced composite materials; Elastic wave; Multiple scattering; Dispersion relation; Stop band; Periodic composites; Random composites

1. Introduction

Propagation of elastic waves in composite materials is one of the key issues regarding their dynamic performance and nondestructive characterization. Ultrasonic nondestructive evaluation of composite materials relies on the information of their wave velocity or attenuation properties obtained by the analysis of transmitted or reflected ultrasonic signals (Kline, 1992). To enhance the qualitative as well as quantitative understanding of the evaluation principles, it is of importance to gain detailed knowledge on the wave

* Corresponding author. Tel.: +81-52-789-4477; fax: +81-52-789-3909.
E-mail address: biwa@mech.nagoya-u.ac.jp (S. Biwa).

0020-7683/$ - see front matter © 2003 Elsevier Ltd. All rights reserved.
doi:10.1016/j.ijsolstr.2003.09.015

propagation behavior in composites. For fiber-reinforced composite materials, one needs to consider a complex process of multiple scattering that occurs as the incident wave interacts with the fibers.

Multiple scattering of elastic waves in fiber-reinforced composite materials have been considered by many authors, including Bose and Mal (1973, 1974), Varadan et al. (1978, 1986), Datta et al. (1984), Liu and Kriz (1998), Kim (2003) to name but a few. Among them, Yang and Mal (1994), and then Huang and Rokhlin (1995), applied a generalized self-consistent model of fiber composites to the Waterman–Truell multiple scattering theory (Waterman and Truell, 1961) to extend its applicability to moderate fiber volume fractions. Other theories so far formulated include the variational principles (Talbot and Willis, 1983), the differential (incremental) scheme (Beltzer and Brauner, 1987; Biwa et al., 2003), etc, for randomly arranged fiber composites. On the other hand, homogenization techniques based on asymptotic expansions or the Bloch theorem have been applied to wave propagation in composites with regular and periodic fiber arrangements (Nelson and Navi, 1975; Murakami and Hegemier, 1986; Naciri et al., 1994). Such periodic composites recently attract much attention regarding the phononic band gap structures and their acoustic applications (Kushwaha et al., 1993, 1994).

Recently, Cai and Williams (1999a) proposed a numerical simulation technique for large-scale multiple scalar wave scattering in fiber-reinforced composites based on a procedure called scatterer polymerization. In this procedure, a group of several scatterers is successively replaced by a single equivalent scatterer, which enables to perform the computation for many-fiber problems with reasonable computational costs. They demonstrated multiple scattering of a scalar shear wave in a unidirectional composite with square fiber arrangements (Cai and Williams, 1999b,c). This technique is, however, not suitable for examining the wave field within the composite, since the original fiber arrangements are lost in the polymerization procedure.

In order to carry out a more straightforward and detailed analysis of the wave field in fiber/matrix composites, an alternative computational approach is presented in this paper for the multiple scattering problem, where the time-harmonic wave field is expressed in terms of the eigenfunction expansion of the scattered wave associated to each fiber. The expansion coefficients are determined numerically using a collocation technique. In this paper, the shear wave mode with the polarization parallel to the fiber direction is considered, as its scalar wave nature is suitable to delineate the essential features of multiple scattering. The present analysis enables detailed examination of the wave structure in the composite in a direct manner.

In what follows, first the basic formulation of the multiple scattering for the scalar shear wave in unidirectional composites is summarized, and a computational procedure to attack the problem is put forward. As an application of the present technique, the shear wave scattering and the overall wave propagation behavior in unidirectional SiC fiber-reinforced Ti-alloy matrix composites are analyzed. Our attention is first focused on the examples for regular fiber arrangements. Namely, for the square as well as hexagonal fiber arrangements, the wave fields in the composite are demonstrated for different frequencies, and the dispersion relation and the energy transmission behavior are illustrated. In addition, a case with irregular distribution of fibers is also treated in order to demonstrate the applicability of the present scheme to arbitrary fiber arrangements. The results obtained by the present analysis are discussed in comparison to the results based on the above-mentioned multiple scattering model by Yang and Mal (1994).

2. Fundamental equations of multiple wave scattering

In this section, the basic equations for the multiple scattering of scalar wave in two-dimensional composite media are recapitulated, which are common to the above-mentioned foregoing works, e.g. Varadan et al. (1978), Datta et al. (1984). The present paper deals with a unidirectional fiber-reinforced composite material consisting of an isotropic elastic infinite matrix (density ρ_1, shear modulus μ_1) with N circular,

isotropic elastic fibers of radius a (density ρ_2, shear modulus μ_2), as schematically shown in Fig. 1. In the x_1–x_2 plane shown in Fig. 1, the fibers can take an arbitrary arrangement. When the plane transverse (shear) wave with polarization parallel to the fibers is incident in the positive x_1 direction, the wave field within the x_1–x_2 plane can be formulated in the framework of scalar wave propagation, since no mode conversion occurs at wave scattering by each fiber and the only nontrivial displacement components are in the x_3 direction.

In the absence of body forces, the equation of motion for the displacement u in the x_3 direction reads

$$\left(\frac{\partial^2}{\partial x_1^2}+\frac{\partial^2}{\partial x_2^2}\right)u-\frac{1}{c_\alpha^2}\frac{\partial^2 u}{\partial t^2}=0, \tag{1}$$

for the matrix ($\alpha=1$) and for the fibers ($\alpha=2$), respectively, where $c_\alpha=(\mu_\alpha/\rho_\alpha)^{1/2}$ is the shear wave speed in the respective medium. As a monochromatic wave motion with temporal dependence $\exp(-\mathrm{i}\omega t)$ is solely considered (ω: angular frequency), Eq. (1) reduces to the scalar Helmholtz equation for $u(x_1,x_2)$;

$$\left(\frac{\partial^2}{\partial x_1^2}+\frac{\partial^2}{\partial x_2^2}\right)u+k_\alpha^2 u=0, \tag{2}$$

where k_α is the wave number in each medium, i.e. $k_\alpha=\omega/c_\alpha$ ($\alpha=1,2$). Hereafter, the time-dependent factor $\exp(-\mathrm{i}\omega t)$ is omitted in all relevant physical quantities and the complex notation is used, where real parts are to represent the actual wave field. The incident wave is assumed to be a plane wave with unit amplitude propagating in the positive x_1 direction, expressed in complex notation as

$$u^{\mathrm{inc}}(\mathbf{r})=\exp(\mathrm{i}k_1\mathbf{i}_1\cdot\mathbf{r}), \tag{3}$$

where $\mathbf{r}$ is the position vector and $\mathbf{i}_1$ the unit vector in the x_1 direction.

In the presence of N fibers, the wave field in the matrix is written as

$$u(\mathbf{r})=u^{\mathrm{inc}}(\mathbf{r})+\sum_{i=1}^{N}u_i^{\mathrm{sca}}(\mathbf{r}), \tag{4}$$

where $u_i^{\mathrm{sca}}(\mathbf{r})$ denotes the wave scattered by the ith fiber. Since $u_i^{\mathrm{sca}}(\mathbf{r})$ is an out-going diverging solution to Eq. (2), it can be expanded using the eigenfunctions in local polar coordinates as (Pao and Mow, 1971)

$$u_i^{\mathrm{sca}}(\mathbf{r})=\sum_{n=-\infty}^{\infty}b_n^i H_n(k_1|\mathbf{r}-\mathbf{r}_i|)\exp(\mathrm{i}n\theta_i), \tag{5}$$

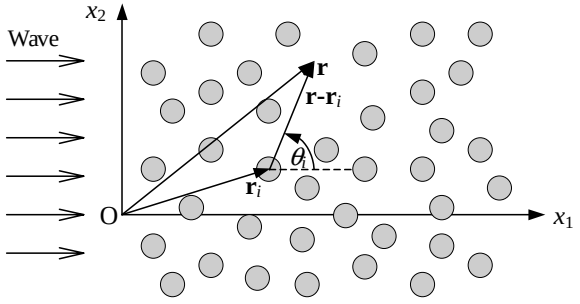

Fig. 1. Schematic representation of a unidirectional fiber-reinforced composite.

where $\mathbf{r}_i$ is the position of the center of the ith fiber, and θ_i is the angular coordinate when $\mathbf{r}$ is viewed from $\mathbf{r}_i$ (Fig. 1), and $H_n(\cdot)$ is the nth order Hankel function of the first kind. The expansion coefficients b_n^i $(n = 0, \pm1, \pm2, \ldots)$ are yet unknown parameters.

The wave field near $\mathbf{r}_i$ that would result if the ith fiber were not there is referred to as the exciting field to that fiber, and is expressed as

$$u_i^{\mathrm{exc}}(\mathbf{r}) = u^{\mathrm{inc}}(\mathbf{r}) + \sum_{\substack{j=1 \\ j\neq i}}^{N} u_j^{\mathrm{sca}}(\mathbf{r}) = \sum_{n=-\infty}^{\infty} a_n^i J_n(k_1|\mathbf{r} - \mathbf{r}_i|)\exp(\mathrm{i}n\theta_i), \tag{6}$$

since it is a solution to Eq. (2) with no singularity at $\mathbf{r}_i$, where a_n^i $(n = 0, \pm1, \pm2, \ldots)$ are the expansion coefficients and $J_n(\cdot)$ is the nth order Bessel function of the first kind. The ith fiber is irradiated by the exciting field u_i^{exc} and gives rise to the scattered wave u_i^{sca}. It is known that for circular cylindrical fibers bonded to the matrix, the coefficients in their expansions can be related linearly as

$$b_n^i = T_n a_n^i, \quad T_n = \frac{\mu_1 k_1 J_n'(k_1 a) J_n(k_2 a) - \mu_2 k_2 J_n(k_1 a) J_n'(k_2 a)}{\mu_2 k_2 H_n(k_1 a) J_n'(k_2 a) - \mu_1 k_1 H_n'(k_1 a) J_n(k_2 a)}, \tag{7}$$

where the prime ($'$) denotes differentiation of the Bessel or Hankel functions with respect to their arguments. Here, T_n are the components of the so-called T-matrix (Waterman, 1969), which becomes diagonal for circular fibers.

Likewise, the refracted wave field inside the ith fiber is expanded as

$$u_i^{\mathrm{ref}}(\mathbf{r}) = \sum_{n=-\infty}^{\infty} c_n^i J_n(k_2|\mathbf{r} - \mathbf{r}_i|)\exp(\mathrm{i}n\theta_i), \tag{8}$$

$$c_n^i = S_n a_n^i, \quad S_n = \frac{J_n(k_1 a) + T_n H_n(k_1 a)}{J_n(k_2 a)}. \tag{9}$$

The relations in Eqs. (7) and (9) stem from the requirement of the continuity of the displacement and the shear traction at the fiber–matrix interface.

From the above equations, the expansion coefficients for the scattered, exciting and refracted waves can be determined, which in turn give the wave field in the composite. For a large number of fibers, however, it is intractable to seek for an analytical solution of the above system of equations. In most of the foregoing multiple scattering theories (Sobczyk, 1985; Varadan et al., 1989), the positions of the fibers are assumed as random variables and the configurational average of the wave field is considered. Assumptions such as the quasi-crystalline approximation or the total wave approximation are then employed to truncate the infinite hierarchy of the resulting set of integral equations, yielding some well known formulae (Foldy, 1945; Waterman and Truell, 1961). In the present paper, the above equations are solved directly using a numerical collocation technique. Therefore, the present procedure as described below is capable of dealing with regular or irregular fiber arrangements explicitly.

3. Computational procedure

In order to solve the equations formulated above, the infinite sums of the eigenfunction expansions in Eqs. (5), (6) and (8) are truncated at a finite level, i.e. $n = 0, \pm1, \pm2, \ldots, \pm n_{\max}$ The integer parameter $n_{\max}$ is chosen as an appropriate number depending on each specific problem. When the wavelength of the

incident wave is large compared to the fiber diameter, it is often sufficient to take the sums up to small $n_{\max}$.

When Eqs. (3), (5) and (7) are substituted into Eq. (6), one obtains

$$\sum_{n=-n_{\max}}^{n_{\max}} a_n^i J_n(k_1|\mathbf{r}-\mathbf{r}_i|)\exp(\mathrm{i}n\theta_i) = \exp(\mathrm{i}k_1\mathbf{i_1}\cdot\mathbf{r}) + \sum_{\substack{j=1\\ j\neq i}}^{N}\sum_{m=-n_{\max}}^{n_{\max}} T_m a_m^j H_m(k_1|\mathbf{r}-\mathbf{r}_j|)\exp(\mathrm{i}m\theta_j), \tag{10}$$

which constitutes a set of equations in terms of the $N\times(2n_{\max}+1)$ expansion coefficients of the exciting field a_n^i $(i=1,2,\ldots,N;\ n=0,\pm1,\pm2,\ldots,\pm n_{\max})$. In the present analysis, a collocation method is employed to obtain a linear set of $N\times(2n_{\max}+1)$ equations to determine these coefficients, i.e., by evaluating the coefficients of a_n^i in Eq. (10) at $(2n_{\max}+1)$ points for each of N fibers. In the present modeling, $(2n_{\max}+1)$ collocation points are taken at equally distanced positions on the circular boundary between the matrix and each fiber.

When analyzing wave propagation in fiber composites, one of our main interests lies in the wave structure along the propagation path. To keep the computation tractable while retaining enough degrees of freedom in the propagation direction, it appears reasonable to assume certain periodicity of the fiber arrangement in the direction perpendicular to the propagation direction. To this purpose, as shown in Fig. 2, the fiber arrangement in the composite is assumed to be a consequence of building up "fundamental" blocks in the x_2 direction. A fundamental block has a dimension of $L\times H$ and contains N fibers, in which the arrangement of the fibers can be either regular or random. The whole composite is constructed by repeating these blocks in the vertical direction, so that infinite fibers are distributed within the region $0<x_1<L$.

In this situation, it is expected that the wave field in the composite becomes periodic in the x_2 direction with period H. Therefore, the exciting field for a generic fiber in a fundamental block becomes identical to those for the corresponding fibers in other blocks. When Eq. (10) is applied to the whole composite and a use is made of this periodicity nature, the equations for the whole system can be reduced to

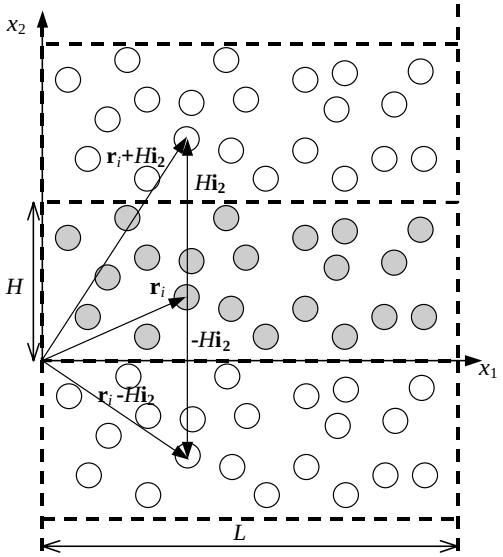

Fig. 2. Periodic structure of fundamental blocks.

$$\sum_{n=-n_{\max}}^{n_{\max}} a_n^i J_n(k_1|\mathbf{r}-\mathbf{r}_i|)\exp(\mathrm{i}n\theta_i)$$
$$= \exp(\mathrm{i}k_1\mathbf{i}_1\cdot\mathbf{r}) + \sum_{p=-\infty}^{\infty}\sum_{\substack{j=1\\ j\neq i}}^{N}\sum_{m=-n_{\max}}^{n_{\max}} T_m a_m^j H_m(k_1|\mathbf{r}-(\mathbf{r}_j+pH\mathbf{i}_2)|)\exp(\mathrm{i}m\theta_{jp})$$
$$+ \sum_{\substack{p=-\infty\\ p\neq 0}}^{\infty}\sum_{m=-n_{\max}}^{n_{\max}} T_m a_m^i H_m(k_1|\mathbf{r}-(\mathbf{r}_i+pH\mathbf{i}_2)|)\exp(\mathrm{i}m\theta_{ip}), \tag{11}$$

where $\mathbf{i}_2$ is the unit vector in the x_2 direction, and θ_{ip} is the angular coordinate when the position $\mathbf{r}$ is viewed from the fiber at $\mathbf{r}_i + pH\mathbf{i}_2$, corresponding to the ith fiber in a block translated by p blocks in the x_2 direction ($p = 0, \pm1, \pm2, \ldots$). Thus the equations for infinite fibers in the region $0 < x_1 < L$ of the composite have been represented in terms of the expansion coefficients for the N fibers in one fundamental block covering $0 < x_1 < L$, $0 < x_2 < H$.

In this formulation, the wave field in the composite is characterized by $N \times (2n_{\max} + 1)$ parameters. In the case when $n_{\max}$ can be chosen as a small number (i.e. when the frequency under question is relatively low), this is considered to be particularly advantageous from a computational viewpoint, compared to other numerical methods such as finite element or boundary element techniques where the whole regions or the fiber–matrix boundaries need to be discretized into many small elements.

If once the coefficients a_n^i are determined, the wave field in the composite can be calculated as

$$u(\mathbf{r}) = \exp(\mathrm{i}k_1\mathbf{i}_1\cdot\mathbf{r}) + \sum_{i=1}^{N}\sum_{n=-n_{\max}}^{n_{\max}} T_n a_n^i \sum_{p=-\infty}^{\infty} H_n(k_1|\mathbf{r}-(\mathbf{r}_i+pH\mathbf{i}_2)|)\exp(\mathrm{i}n\theta_{ip}) \tag{12}$$

in the matrix, and

$$u_i^{\mathrm{ref}}(\mathbf{r}) = \sum_{n=-n_{\max}}^{n_{\max}} S_n a_n^i J_n(k_2|\mathbf{r}-\mathbf{r}_i|)\exp(\mathrm{i}n\theta_i) \tag{13}$$

in the fiber at $\mathbf{r}_i$.

4. Application to periodic composites

4.1. Computational model

The computational procedure proposed above is now applied to analyze the wave scattering and the overall wave propagation in a unidirectional composite consisting of Ti-alloy matrix and SiC fibers. The material properties of these constituents are summarized in Table 1. Effects of the coating layer or the fiber/matrix debonding damage in this composite system have been analyzed previously (Rokhlin et al., 1995;

Table 1
Material parameters used for numerical analysis

Matrix (Ti-alloy)		Fiber (SiC)	
μ_1 (GPa)	ρ_1 (kg/m^3)	μ_2 (GPa)	ρ_2 (kg/m^3)
45	5400	177	3200

Biwa and Shibata, 2000). In this paper, however, such effects are ignored to keep simplicity of the analysis: the fibers are directly bonded to the matrix and the fiber radius is set as 71 μm (Rokhlin et al., 1995). The extension to the case involving the finite compliance of the fiber–matrix interface is not a difficult task as it can be incorporated by modification of the T-matrix formulation.

In this chapter, the composites with regular and periodic fiber arrangements are examined. Two types of fiber arrangements are considered in the fundamental block. The first case is a regular square arrangement with 80 fibers in the x_1 direction and 2 fibers in the x_2 direction, Fig. 3(a). The second case is a hexagonal arrangement, having 160 fibers likewise in the fundamental block as in Fig. 3(b). By changing the fiber spacing and the total size of the fundamental block, the volume fraction of the fibers in a fundamental block is varied in the numerical model.

When the frequency is sufficiently low and the wavelength is much larger than the fiber radius, the eigenfunction expansion of the wave field only requires a few leading terms. As the wavelength becomes shorter (as the frequency becomes higher), an increasing number of terms need to be included in the analysis. The necessity of higher-order terms also depends on the acoustic mismatch between the matrix and fibers. After preliminary numerical experiments, the required number of the n-terms was estimated as a function of the frequency. As a result, it has been found for the present SiC/Ti-alloy composite system that for a frequency lower than 4 MHz it is numerically sufficient to take $n_{\max}$ to be 2. For an intermediate range of 4–10 MHz, $n_{\max}$ is taken as 3 or 4, while for the range of 10–15 MHz, $n_{\max}$ is taken as 5 or 6. For a typical example, Fig. 4 shows a part of the total wave field $\mathrm{Re}[u]$ along the x_1-axis at $x_2 = H/2$ for different truncation levels of $n_{\max}$ for the square fiber arrangement and for the frequency of 5 MHz, where the truncation at $n_{\max} = 3$ is shown to be sufficient.

The influence of truncating the sums over p in Eqs. (11)–(13) was also examined, and the summation up to at least ±100, ±200 and ±500 was typically required from a numerical viewpoint for the above three frequency ranges, respectively, for the particular composite system analyzed here. The level of truncation was verified on a numerical basis by confirming satisfactory agreement between the numerical results obtained with different levels of truncation. Furthermore, the numerical results were found to be insensitive to the particular choice for the location of the equally spaced collocation points on the fiber–matrix boundaries.

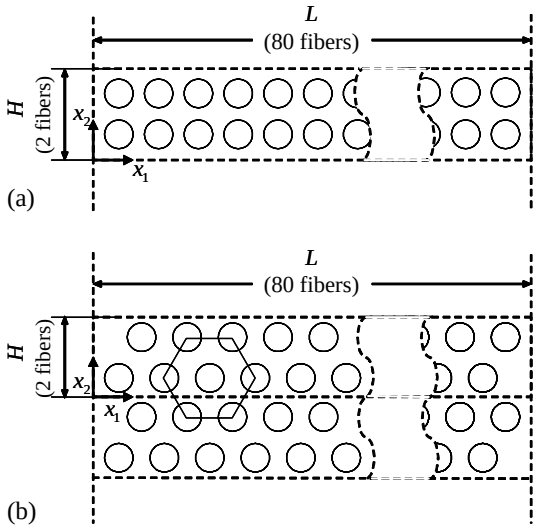

Fig. 3. Regular fiber distributions in a fundamental block, (a) square arrangement, (b) hexagonal arrangement.

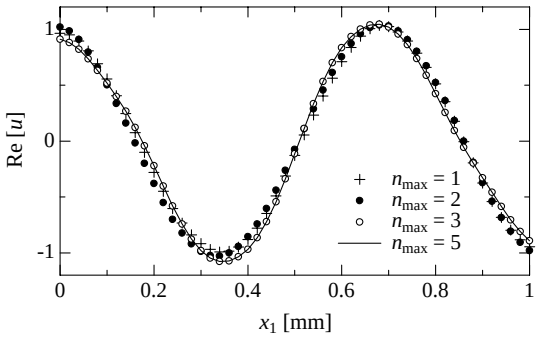

Fig. 4. The wave field Re[u] along the x_1-axis at $x_2 = H/2$ for different truncation levels of $n_{\max}$ for the square fiber arrangement and for the frequency of 5 MHz.

4.2. Wave field in the composite

For the unidirectional SiC/Ti-alloy composite, the wave field is computed by Eq. (12) (in the matrix) and Eq. (13) (in the fibers) after determining the eigenfunction expansion coefficients by the numerical collocation procedure described above. For the fiber volume fraction $\phi = 0.25$, the wave fields in the composite given by Re[u] are shown at different frequency levels, for the square fiber arrangement in Fig. 5 and for the hexagonal fiber arrangement in Fig. 6. For this fiber volume fraction and the assumed fiber radius of 0.071 mm, the center-to-center fiber spacing is about 0.25 and 0.27 mm for the square and hexagonal fiber arrangements, respectively.

Figs. 5(a) and 6(a) correspond to the frequency $f = \omega/(2\pi)$ of 1 MHz, for which the wavelength in the matrix is $c_1/f \cong 2.89$ mm (the ratio of the fiber radius to the wavelength $fa/c_1 \cong 0.025$), and the wave fields are shown for a region $0 < x_1 < 20$ mm and $0 < x_2 < 0.5$ mm that approximately covers one fundamental block. Figs. 5(b) and 6(b) for 4 MHz, $c_1/f \cong 0.72$ mm ($fa/c_1 \cong 0.1$), are for one quarter of the fundamental block, $0 < x_1 < 5$ mm, and Figs. 5(d) and 6(d) for 10 MHz, $c_1/f \cong 0.29$ mm ($fa/c_1 \cong 0.25$), are for one tenth of it, $0 < x_1 < 2$ mm. Likewise, Fig. 5(c) for 6.6 MHz ($fa/c_1 \cong 0.16$) corresponds to the region $0 < x_1 < 4$ mm, and Fig. 6(c) for 8.4 MHz ($fa/c_1 \cong 0.21$) to $0 < x_1 < 3$ mm. In this way, more or less similar numbers of the wavelengths are illustrated for all frequencies in Figs. 5 and 6.

From Figs. 5(a) and 6(a), it is readily found that at the lowest frequency of 1 MHz, the wave fields in the composite for square and hexagonal fiber arrangements do not differ from each other very much. Furthermore, they appear to be an essentially sinusoidal plane wave, indicating the negligible influence of the fiber arrangement on the wave field at sufficiently low frequency. However, as the frequency becomes higher, the wave fields show different appearances depending on the fiber arrangement, and are no longer simple plane waves. Especially in the high frequency cases of Figs. 5(d) and 6(d), the wave fields are fairly complex as the fiber spacing is comparable to the wavelength. In these plots, some of the fiber positions can be visibly identified as relatively flat spots since the fibers are stiffer than the matrix.

It should be noted that while Fig. 5(a), (b) and (d) as well as Fig. 6(a), (b) and (d) show the behavior of propagating waves with spatial periodicity, Figs. 5(c) and 6(c) exhibit completely different characteristics. Namely, at 6.6 MHz in the case of square arrangement and at 8.4 MHz in the case of hexagonal arrangement, the wave amplitude appears to decay drastically as one goes to the positive x_1 direction. These frequencies correspond to the so-called stop bands, which will be discussed in more detail in the following sections.

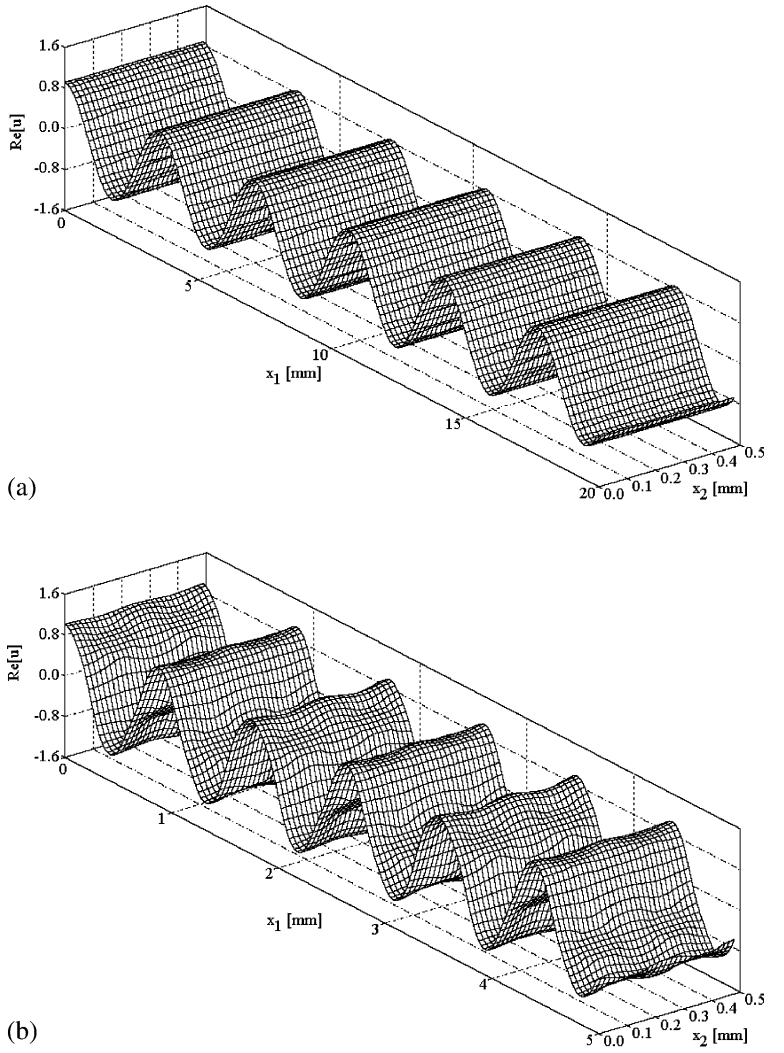

Fig. 5. Wave field in the composite with square fiber arrangement, $\phi = 0.25$, at (a) 1 MHz ($fa/c_1 \cong 0.025$), (b) 4 MHz ($fa/c_1 \cong 0.1$), (c) 6.6 MHz ($fa/c_1 \cong 0.16$) and (d) 10 MHz ($fa/c_1 \cong 0.25$).

4.3. Dispersion relation

Fig. 7 shows the computed total wave field along the x_1 direction in the composite with the square fiber arrangement, when the frequency is 1 MHz and the fiber volume fraction is $\phi = 0.25$ and 0.5. The curves in Fig. 7 represent the total wave field along the centerline of the fundamental block at $x_2 = H/2$, with the arrows indicating the composite region sandwiched by the two semi-infinite regions of the matrix. These curves are compared to the case of $\phi = 0$ showing the incident wave in the matrix that would result if there were no fibers present. As the fiber volume fraction is increased, the wavelength of the total wave in the composite increases, which means that the phase velocity in the composite increases as the fiber fraction is increased. By fitting these curves with a sinusoidal function or applying the fast Fourier transform (FFT) to them, the wave number in the composite can be identified. This procedure was also applied to other

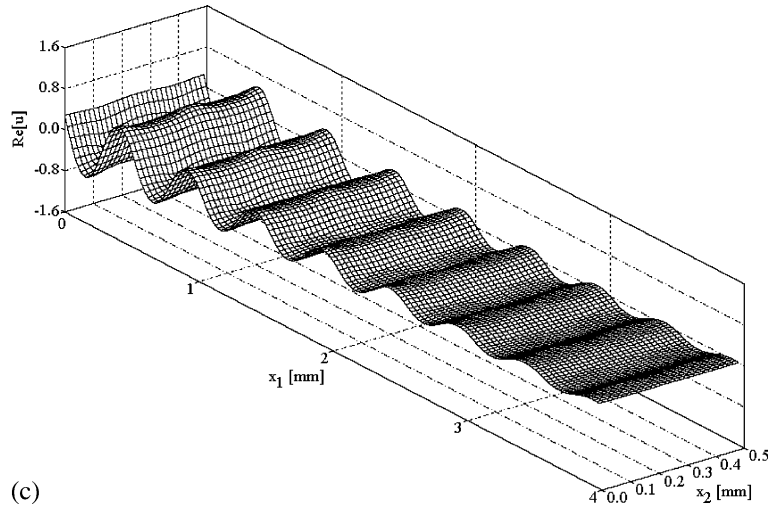

(c)

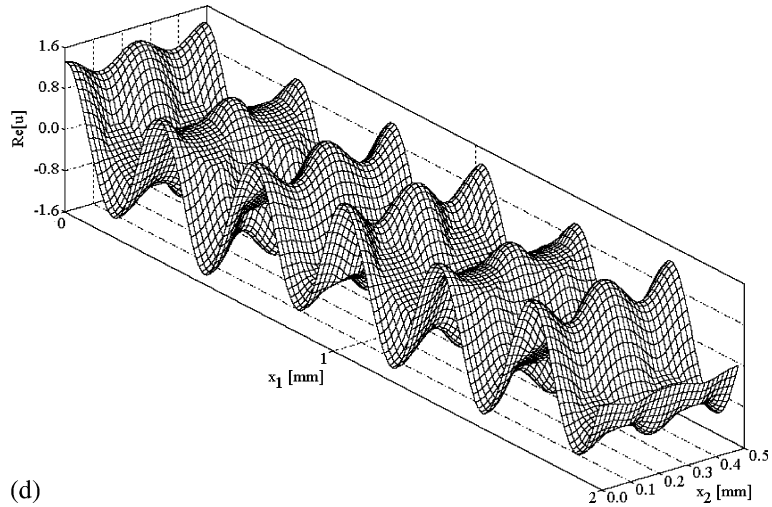

(d)

Fig. 5 (*continued*)

computed wave fields, and the wave number in the composite was obtained as a function of the frequency, for the square as well as for the hexagonal fiber arrangements.

The relation between the so-obtained wave number k and the frequency f is plotted in Fig. 8(a) and (b) for the square and hexagonal fiber arrangements, respectively, and for two different fiber volume fractions. In Fig. 8, the wave numbers are normalized as kd/π, where the center-to-center fiber spacing d is given by

$$d = \sqrt{\frac{\pi}{\phi}}a \tag{14a}$$

for the square arrangement, and by

$$d = \sqrt{\frac{2\pi}{\sqrt{3}\phi}}a \tag{14b}$$

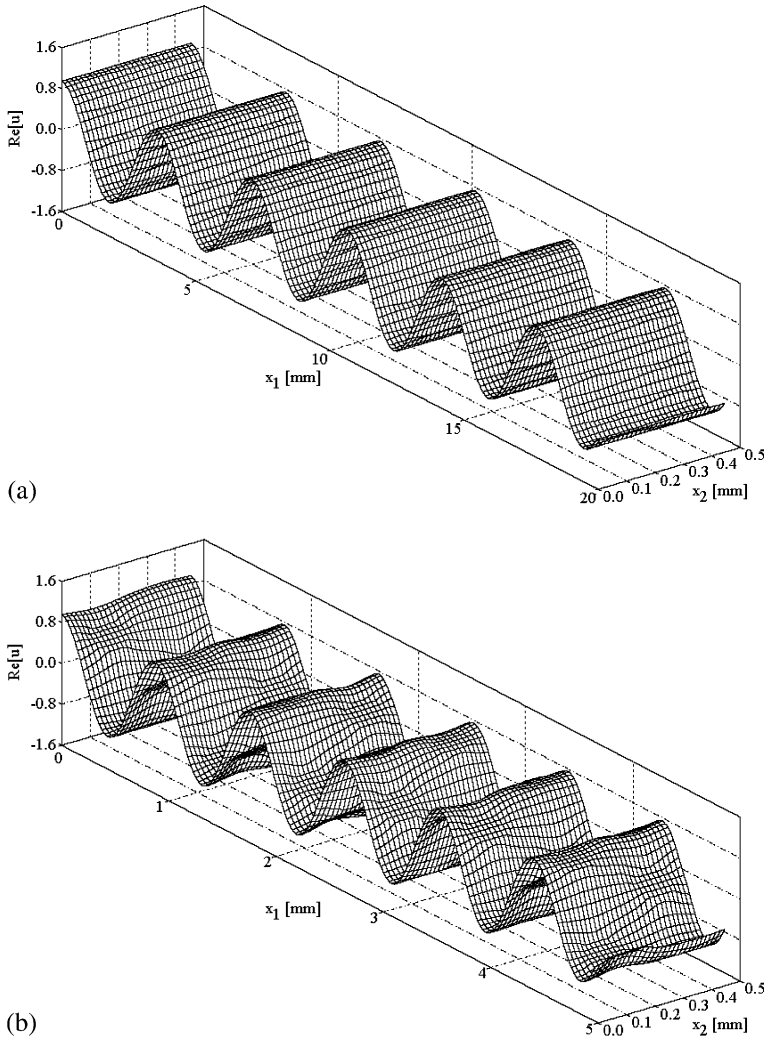

Fig. 6. Wave field in the composite with hexagonal fiber arrangement, $\phi = 0.25$, at (a) 1 MHz ($fa/c_1 \cong 0.025$), (b) 4 MHz ($fa/c_1 \cong 0.1$), (c) 8.4 MHz ($fa/c_1 \cong 0.21$) and (d) 10 MHz ($fa/c_1 \cong 0.25$).

for the hexagonal arrangement, for each fiber volume fraction ϕ. These plots show the dispersion relation of the shear wave in the periodic composite at hand. At some locations of the dispersion curve, however, the wave number appears to stagnate against increasing frequency. In other words, the frequency exhibits a finite jump at these wave numbers.

For the square arrangement, this has occurred at $kd = \pi$ and $kd = 2\pi$, corresponding to the Bragg reflection well known in solid state physics (Kittel, 1976), from the neighboring fiber planes normal to the propagation direction. For the hexagonal arrangement, the corresponding locations are found at $kd = 4\pi/3$ and $kd = 2\pi$. The former condition corresponds to the Bragg reflection from the fiber planes inclined by $\pi/6$ rad to the propagation direction, while the latter to the reflection from the planes normal to the propagation direction. The frequency ranges giving the above tendency are referred to as stop bands, in common terminology for the wave propagation in periodic systems. The frequencies for Figs. 5(c) and 6(c), where the wave amplitude has been found to decay spatially, are within the stop bands for the composite.

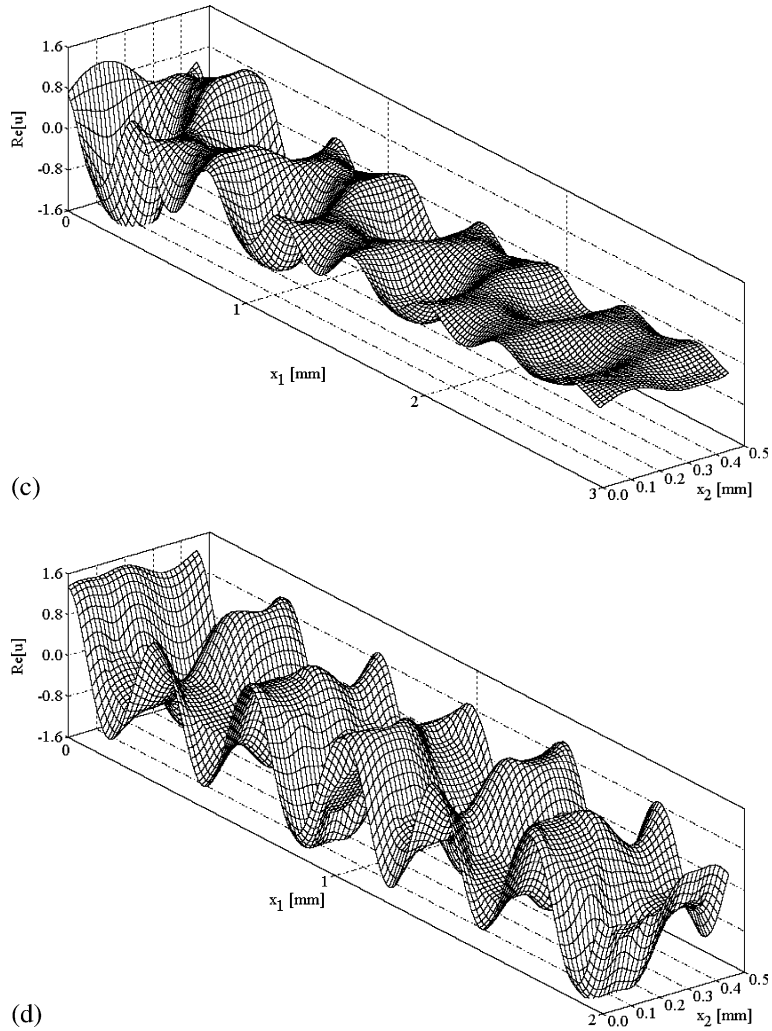

Fig. 6 (*continued*)

4.4. Phase velocity

In Fig. 9(a) and (b), the phase velocity of the composite is plotted as a function of the frequency for the fiber volume fractions $\phi = 0.25$ and 0.5, for the square and hexagonal arrangements, respectively. The phase velocity has been obtained from the dispersion curves in Fig. 8 by the relation $c = \omega/k$ and normalized by the matrix shear wave speed $c_1 \cong 2887$ m/s. It is noted though that within the stop bands indicated by arrows the wave ceases to possess a propagating nature and the usage of the term of phase velocity becomes somewhat inadequate. As shown in Fig. 9, the phase velocity shows substantial fluctuation in the vicinity of the stop bands. This feature is akin to the experimental results by Kinra and Ker (1983) and Henderson et al. (2001) for the longitudinal wave propagation in periodic particle-reinforced composites.

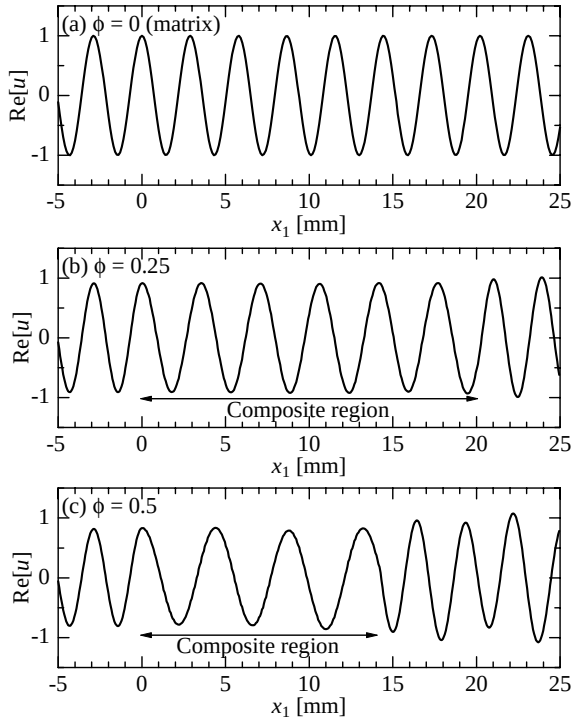

Fig. 7. Wave field along the propagation direction (at $x_2 = H/2$) in the composite with square fiber arrangement at 1 MHz, for $\phi =$ (a) 0, (b) 0.25 and (c) 0.5. The arrows denote the region occupied by the composite.

According to the multiple scattering theory by Waterman and Truell (1961), the effective complex wave number k_{eff} of the mean wave in a random fiber composite is given by

$$\left(\frac{k_{\text{eff}}}{k_1}\right)^2 = \left\{1 - \frac{2in_sF(0)}{k_1^2}\right\}^2 - \left\{\frac{2in_sF(\pi)}{k_1^2}\right\}^2, \tag{15}$$

where $n_s = \phi/(\pi a^2)$ is the number of fibers in a unit volume. In the above expression, the complex quantities $F(0)$ and $F(\pi)$ are the forward and backward scattering amplitudes for a single fiber embedded in the infinite matrix.

The Waterman–Truell formula in Eq. (15) was derived by neglecting the statistical correlation between the scatterer positions in the medium, and its applicability to dense fiber distribution becomes questionable. Based on the concept of a generalized self-consistent model, Yang and Mal (1994) modified the Waterman–Truell theory, and showed that the complex wave number of the composite satisfies

$$1 = \left\{1 - \frac{2in_sF(0)}{k_{\text{eff}}^2}\right\}^2 - \left\{\frac{2in_sF(\pi)}{k_{\text{eff}}^2}\right\}^2. \tag{16}$$

The forward and backward scattering amplitudes in the above expression correspond to a composite scatterer made of the fiber and the annular concentric matrix, which is embedded in an infinite medium having the averaged macroscopic property of the composite. Since these quantities are implicitly dependent on the unknown variable k_{eff}, the above equation is solved iteratively until sufficient convergence is reached. The phase velocity is obtained from the real part of the complex wave number as $c = \omega/\text{Re}[k_{\text{eff}}]$. In Fig. 9, the phase velocities computed by the Yang–Mal model, which considers random fiber arrangements, are compared to the results obtained from the present numerical scattering analysis.

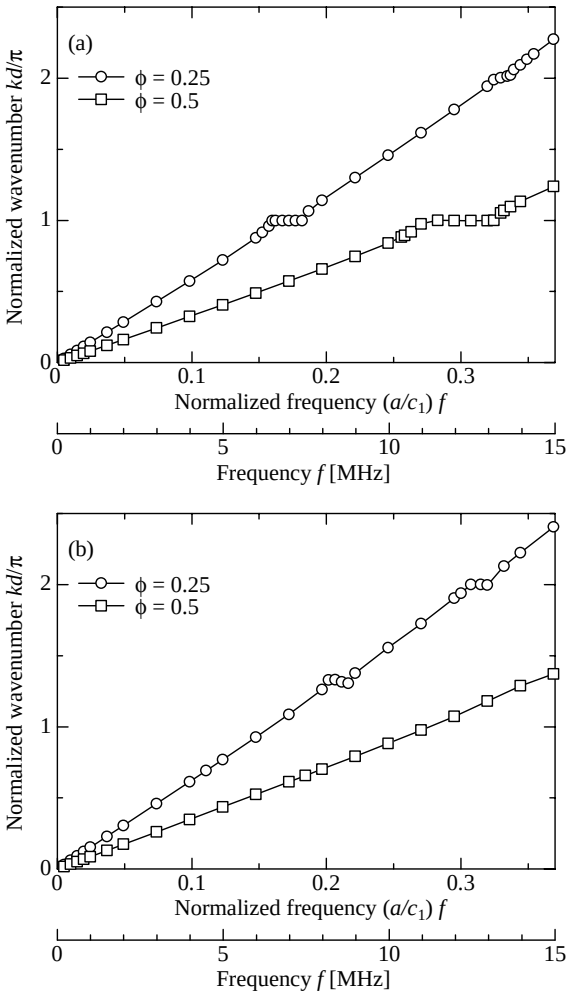

Fig. 8. Dispersion relation between the frequency and the normalized wave number for the composite with $\phi = 0.25$ and 0.5, for (a) square and (b) hexagonal fiber arrangements.

Comparing the results in Fig. 9, it is seen that the Yang–Mal model gives the phase velocities that are close to the present results for both 25% and 50% fiber volume fractions and for both square and hexagonal fiber arrangements, except in the neighborhood of the stop bands identified by the arrows. When the frequency is sufficiently low, the phase velocities of the composite for square and hexagonal fiber arrangements are both indistinguishable from the results by the Yang–Mal model. Thus one recovers that the low frequency (long wavelength) propagation behavior is not sensitive to the fiber arrangement, as already seen in the wave fields shown in Figs. 5(a) and 6(a).

4.5. Energy transmission

To discuss in detail the character of the wave fields shown above, the energy flow associated to the wave motion is considered. When the complex notation is employed to denote the wave displacement u, the time-averaged energy flow across a surface normal to the propagation direction is given by (Pao and Mow, 1971)

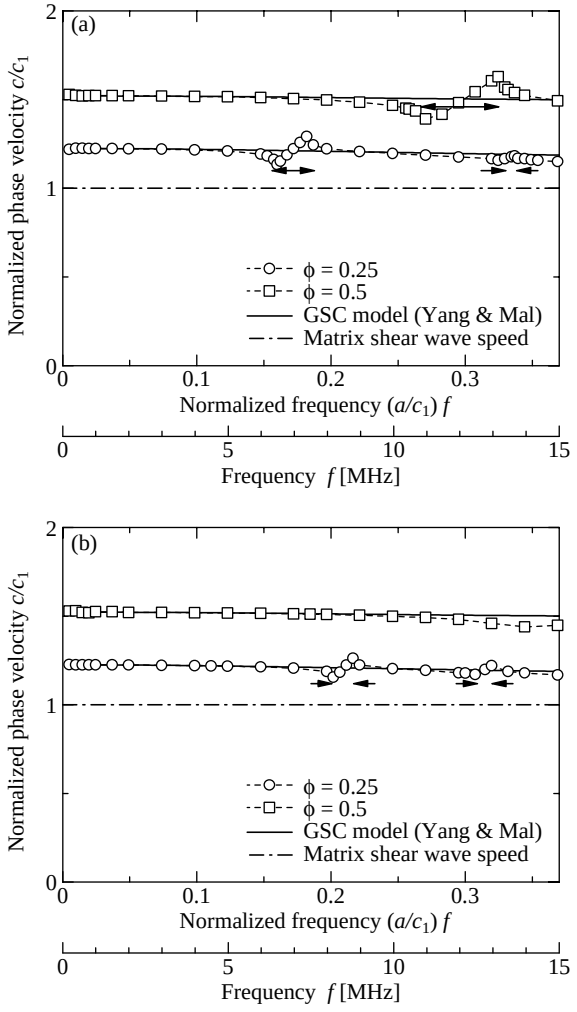

Fig. 9. Frequency dependence of the phase velocity in the composite with (a) square and (b) hexagonal fiber arrangements for $\phi = 0.25$ and 0.5. Symbols: present analysis, solid lines: generalized self-consistent (GSC) model by Yang and Mal (1994), chained lines: matrix shear wave speed. Arrows denote the stop bands.

$$\langle e\rangle(x_1) = -\frac{1}{H}\frac{\mathrm{i}\omega}{4}\int_{-H/2}^{H/2}\left\{\mu\frac{\partial u}{\partial x_1}u^* - \left(\mu\frac{\partial u}{\partial x_1}\right)^* u\right\}\mathrm{d}x_2, \tag{17}$$

when averaged along the x_2 direction, where the shear modulus μ takes on a value of μ_1 or μ_2 depending on the position on the integration path. The superscript (*) denotes the complex conjugate of a complex variable. In the absence of the fibers, the time-averaged energy flow per unit area of the surface normal to the propagation direction is given by

$$\langle e\rangle_0 = \frac{\omega k_1 \mu_1}{2}, \tag{18}$$

when the wave has the unit amplitude. The normalized energy flow $\langle e\rangle(x_1)/\langle e\rangle_0$ then represents the ratio of the transmitted energy flow of the total wave in the composite to that of the incident wave.

Since both the matrix and the fibers are assumed elastic here, the conservation of the energy implies that $\langle e\rangle(x_1)/\langle e\rangle_0$ is independent of x_1. This has been verified in the present numerical analysis within the accuracy of the computation. So the attention is paid to the value of $\langle e\rangle(x_1)/\langle e\rangle_0$ at a single location of $x_1 = 1.1L$ (just past the composite region) in this discussion.

The values of $\langle e\rangle/\langle e\rangle_0$ are thus plotted against the frequency in Fig. 10 for the square and the hexagonal arrangements when the fiber volume fraction is 0.25. In Fig. 10(a) for the square arrangement, it is shown that below 5 MHz roughly the normalized energy flow is almost unity. Therefore, the wave fields shown in Fig. 5(a) (1 MHz) and (b) (4 MHz) corresponds to the case where the energy is fully transmitted in the propagation direction. On the other hand, in a finite frequency band containing the frequency of 6.6 MHz, relating to Fig. 5(c), the level of the energy flow is seen to be null. This indicates that the wave field in Fig. 5(c) corresponds to a standing wave rather than a propagating wave. In fact, an inspection of the time-dependent wave fields $\mathrm{Re}[u\exp(-\mathrm{i}\omega t)]$ for different t has revealed that at 6.6 MHz the particle points in the entire domain move in phase. At 10 MHz, Fig. 5(d), the wave has recovered a propagating nature that transports the full wave energy. The two stop bands shown in Fig. 10(a) coincides with the frequency regions with constant wave numbers at $kd = \pi$ and 2π in Fig. 8(a).

A similar trend can be seen in Fig. 10(b) for the hexagonal case, which confirms that the wave fields at 1 MHz, Fig. 6(a), and 4 MHz, Fig. 6(b), are fully propagating ones, while that at 8.4 MHz, Fig. 6(c), is of a

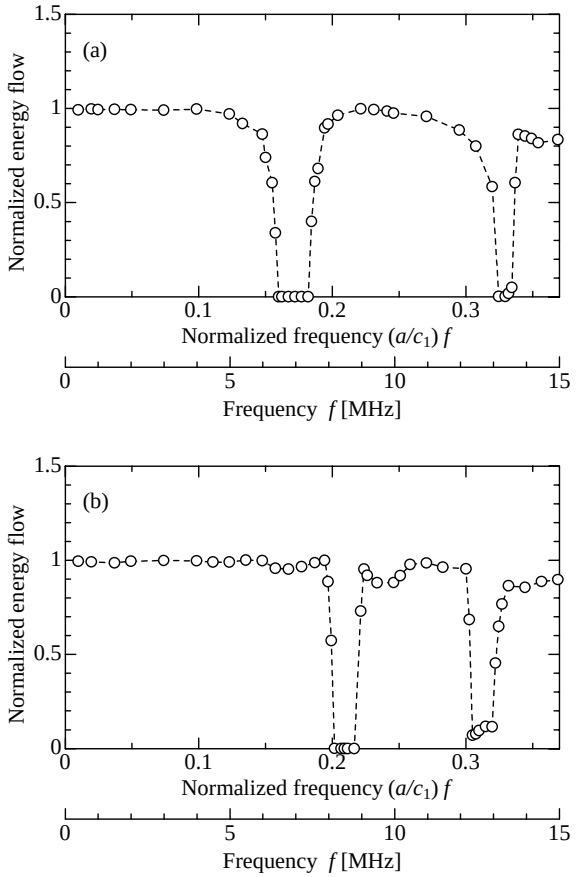

Fig. 10. Variation of the normalized energy transmission with the frequency in the composite with (a) square and (b) hexagonal fiber arrangements.

standing-wave nature. The wave field at 10 MHz shown in Fig. 6(d) corresponds to a pass band, though the energy transmission ratio is not unity but about 0.88. The two stop bands in Fig. 10(b) correspond to the wave numbers $kd = (4/3)\pi$ and 2π as indicated in Fig. 8(b). In the second stop band in Fig. 10(b), it is seen that the energy transmission does not completely vanish but a small portion of the energy is transmitted to the forward direction. In order to fully interpret such characteristics, computations of the band gap structure for the whole Brillouin zone as presented by Kushwaha et al. (1993) seem more appropriate.

In passing, it is noted that the computation of the energy transmission for finer frequency divisions has shown an oscillatory behavior especially near the stop bands, as demonstrated in Fig. 11. In the previous figure (Fig. 10), such oscillations were not apparent as relatively coarse frequency intervals were employed to outline the overall behavior. Fig. 11 compares the oscillatory frequency dependence of the energy transmission near the first stop band of the square arrangement (5–9 MHz), for the present composite model ($L = 20.2$ mm, 80×2 fibers) and for another model with shorter L ($L = 6.54$ mm, 26×6 fibers) with the same fiber volume fraction, $\phi = 0.25$. The frequency intervals of these oscillations are well approximated by $c_1/(2L)$, indicating an effect due to the finite length of the composite region L employed in the computational modeling. It is then expected that these oscillation tend to vanish for the infinitely extended composite with complete periodicity.

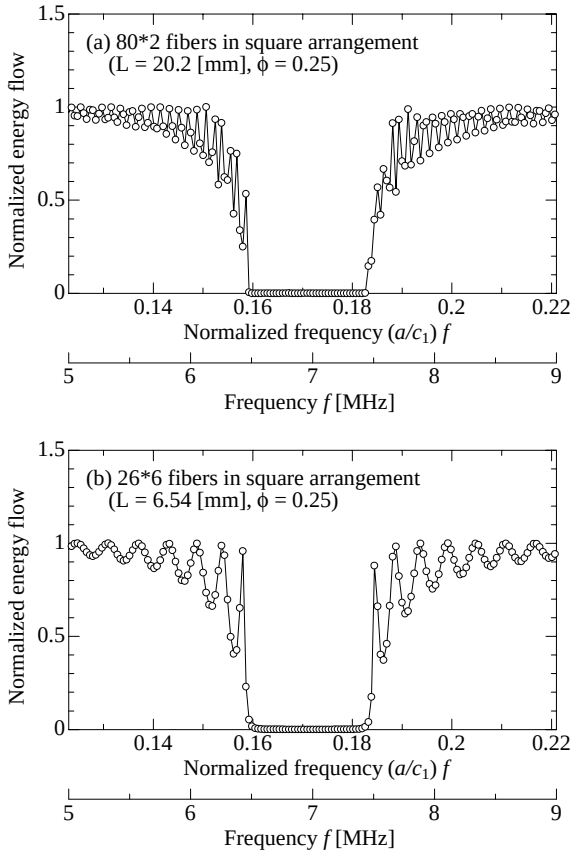

Fig. 11. Frequency dependence of the normalized energy transmission near the first stop band for the square arrangement with $\phi = 0.25$, for (a) the composite with $L = 20.2$ mm and (b) the composite with $L = 6.54$ mm.

5. Application to a random composite

5.1. Computational model

As stated before, the present computational scheme is capable of dealing with arbitrary fiber arrangements in the fundamental block. The results for periodic arrangements demonstrated above have recovered some features pertinent to the wave propagation in periodic systems. In this chapter, some examples are illustrated for the wave propagation characteristics in a composite with random fiber distribution.

In the examples in the previous chapter, the height of the fundamental block H corresponded to two fiber arrays (Fig. 3) taking advantage of the periodic nature of the fiber arrangement. In order to model a random distribution while to keep the computational demand in a reasonable range, the fundamental block of the dimension $L = 6.532$ mm and $H = 1.562$ mm is employed. Within this block, total of 162 fibers are arranged randomly according to a numerical algorithm called random sequential adsorption (RSA) (Feder, 1980) with a supplementary condition that the distance between two neighboring fiber centers meets $|\mathbf{r}_i - \mathbf{r}_j| \geqslant 2.01a$ $(i \neq j)$, as shown in Fig. 12. The fibers located near the boundaries $x_2 = 0$ and $x_2 = H$ are treated by the periodicity requirement common in RSA. This results in the fiber volume fraction $\phi = 0.25$ that is fixed in the analysis of this chapter.

The arrangement in Fig. 12 is considered to be one realization of random fiber distributions. In order to extract the characteristics of the mean wave or the so-called coherent wave (Tourin et al., 2000), computations are required for many of such arrangements. The purpose of this chapter is not to seek for this. Instead, only one realization of Fig. 12 is employed to compute the wave propagation behavior (the wave field, the phase velocity and the energy transmission) of a random composite and to show major differences from the periodic composites shown above.

The material properties of the matrix and the fiber are the same as in Table 1. For the fixed fiber distribution of Fig. 12, the frequency is changed from 0 to 10 MHz ($0 < (a/c_1)f < 0.25$ roughly). It is noted that in a random composite, the fiber-to-fiber distance is not a fixed length but distributed in a certain range. As seen in Fig. 12, some of the fibers are arranged very close to each other. Due to this nature, the truncation levels of the parameters such as $n_{\max}$ have been validated numerically again for each frequency, and higher values are eventually employed than in the corresponding cases of periodic arrangements shown above.

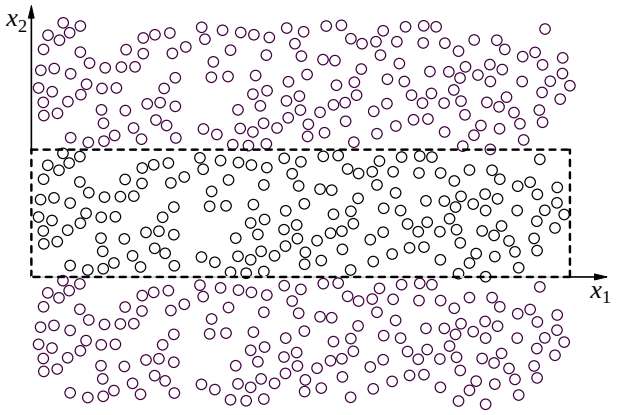

Fig. 12. Random fiber arrangement in the fundamental block (shown by the broken lines) used in the numerical analysis, together with neighboring blocks containing the same fiber arrangement.

5.2. Wave field in the composite

The wave fields corresponding to Figs. 5 and 6 are shown in Fig. 13 for the random composite when the frequency is 1 MHz ($(a/c_1)f \cong 0.025$), 4 MHz ($(a/c_1)f \cong 0.1$) and 7 MHz ($(a/c_1)f \cong 0.175$). For these three frequencies, the wave field $\mathrm{Re}[u]$ in the fundamental block is demonstrated. Fig. 13(a) for 1 MHz shows a sinusoidal plane wave similar to the corresponding periodic cases, Figs. 5(a) and 6(a), indicating again the insensitivity of the long wavelength propagation characteristics to the detailed fiber arrangement. Note again that the fiber locations can be identified visually as discrete spots.

The case with 4 MHz, Fig. 13(b), shows considerable deviation from sinusoidal plane wave forms. This is in contrast to the periodic cases for the same frequency, Figs. 5(b) and 6(b), and partly attributed to the irregular nature of the fiber arrangement. Also, in the random arrangement, many of the fibers are located closer to each other than in the periodic cases, so the local interaction among the fibers may be more prominent in the random case.

In Fig. 13(c), the wave field for 7 MHz is shown. This wave field is considered to be the outcome of significant scattering from each of the fibers arranged irregularly. In particular, some high peaks are seen near the left boundary of the fundamental block. The net time-averaged energy flow in the propagation direction at this frequency is less than 40% of that for the incident wave, as shown in Fig. 15 given below. This suggests the presence of substantial back scattering in the composite. Contrary to the periodic composites, however, the scattered waves by the fibers do not interfere constructively in the random composite.

5.3. Phase velocity and energy transmission

The wave number and the phase velocity in the composite have been identified from the computed wave field. To this end, the wave field $\mathrm{Re}[u]$ has been averaged in the x_2 direction, and a similar FFT procedure as used in Section 4 has been employed in order to extract the wave number. Although the local wave number of the computed average wave field varies slightly depending on the spatial position x_1 it is a single wave number of an averaged character that is obtained by the present procedure. The so-obtained dispersion relation has shown more or less linear increase of the wave number with the frequency. Although the considered frequency range contains the first stop bands of the square and hexagonal composites with the same fiber fraction, the result for the random composite has not revealed a frequency region giving a constant wave number that indicates stop bands.

The phase velocity in the random composite computed from the wave number is plotted in Fig. 14 as a function of the frequency, with the theoretical curve by the Yang–Mal model in Eq. (16). In Fig. 14, the computed phase velocity shows a weak fluctuation with the frequency. Note that the vertical length scale is more magnified than Fig. 9 in order to visualize this fluctuation. Besides this fluctuation, the computed values and the Yang–Mal model are shown to be in good agreement for the entire frequency range shown here.

Finally the normalized time-averaged energy flow $\langle e\rangle/\langle e\rangle_0$ at a location of $x_1 = 1.1L$ averaged over the x_2 direction is plotted in Fig. 15 as a function of the frequency. In the frequency range lower than about 2 MHz ($(a/c_1)f < 0.05$), the normalized energy is nearly unity indicating the full transmission of the wave energy in the propagation direction. As the frequency increases, however, the transmitted energy flow ratio decreases significantly, accompanied by a substantial fluctuation due probably to the irregular fiber arrangement. The random composite analyzed here does not show any frequency bands where the wave energy is perfectly cut off. This result shows that the energy transmission behavior is very sensitive to the fiber arrangement.

As an attempt to interpret the result in Fig. 15 from a theoretical point of view, the decay of the wave energy in the random composite is now estimated by the Yang–Mal model. The imaginary part of the effective wave number k_{eff} determined by Eq. (16) gives the attenuation coefficient of the mean wave in the

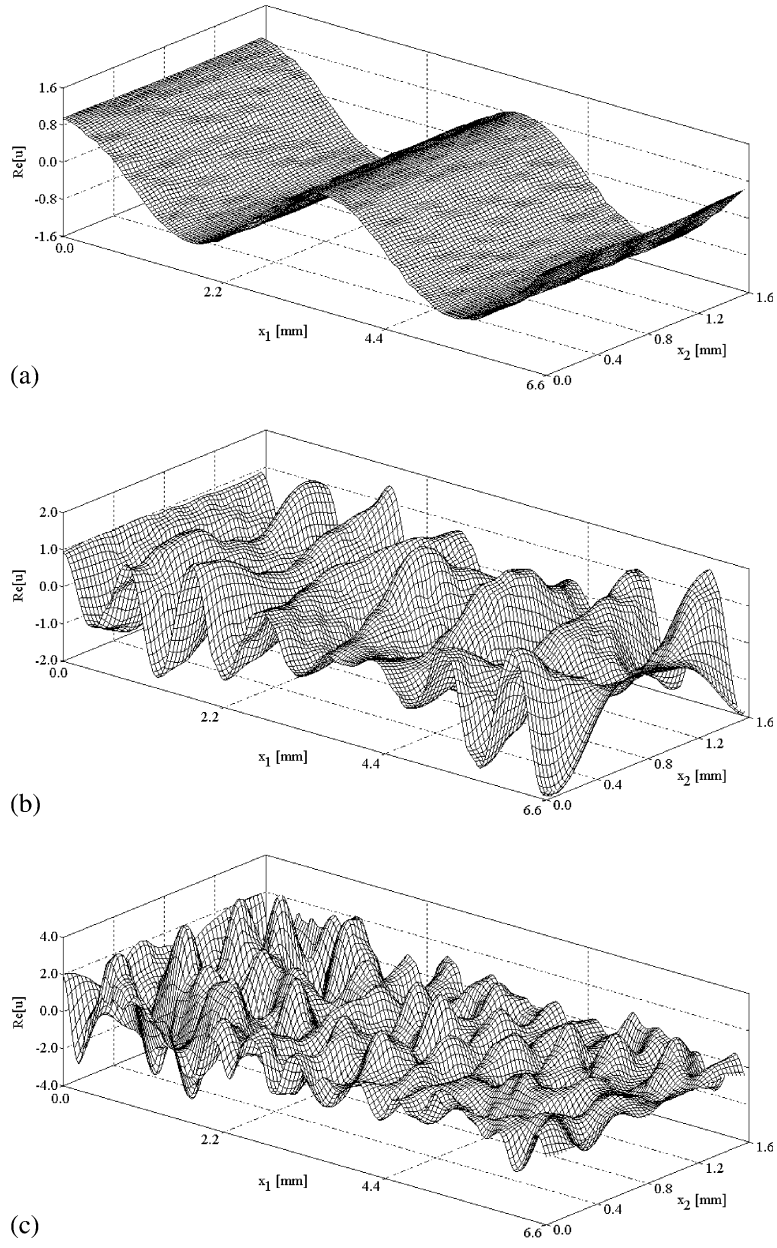

Fig. 13. Wave field in the composite with random fiber arrangement, $\phi = 0.25$, at (a) 1 MHz ($fa/c_1 \cong 0.025$), (b) 4 MHz ($fa/c_1 \cong 0.1$) and (c) 7 MHz ($fa/c_1 \cong 0.175$).

random composite that reflects the scattering loss by the fibers. According to this, the energy of the wave decays as $\exp(-2\mathrm{Im}[k_{\mathrm{eff}}]L)$ when it has propagated the length L of the composite. For $\phi = 0.25$, this quantity is computed from Eq. (16) and superimposed on the computational plots in Fig. 15. While the result by the present analysis exhibits the considerable fluctuation mentioned above, the theoretical curve by the Yang–Mal model shows monotonically-decreasing frequency dependence. It is shown though that

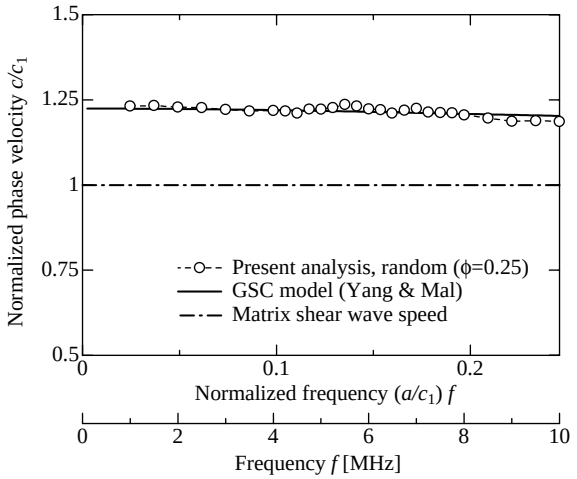

Fig. 14. Frequency dependence of the phase velocity in the random composite for $\phi = 0.25$. Symbols: present analysis, solid line: generalized self-consistent (GSC) model by Yang and Mal (1994), chained line: matrix shear wave speed.

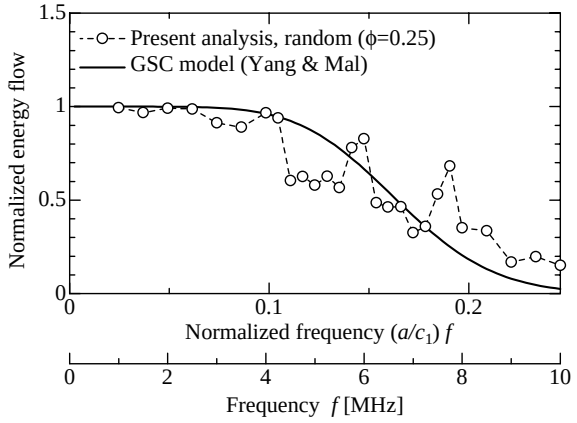

Fig. 15. Variation of the normalized energy transmission with the frequency in the random composite. Symbols: present analysis, solid line: generalized self-consistent (GSC) model by Yang and Mal (1994).

the attenuation predicted by the Yang–Mal model well reproduces the overall trend of the frequency-dependent energy transmission behavior computed in the present analysis.

6. Concluding remarks

A computational procedure for multiple wave scattering in unidirectional fiber-reinforced composite materials has been presented. The present study deals with the time-harmonic equations for the multiple scattering of shear waves polarized parallel with the fibers expressed by the eigenfunction expansion, and a collocation method is used to determine the expansion coefficients. For a practical frequency range relevant to ultrasonic characterization of fiber composites, incorporation of a few leading terms in the expansions can be sufficient, which facilitates the computation substantially together with the assumed periodicity of

the fiber arrangement in the direction normal to the propagation direction. As an example, the shear wave propagation in a unidirectional SiC/Ti-alloy composite has been analyzed, and the wave fields in the composite have been demonstrated for periodic (square and hexagonal) fiber arrangements as well as for a random fiber distribution. The phase velocity and the energy transmission characteristics in the composite have been also illustrated as function of the frequency.

For the periodic fiber arrangements, the stop-band phenomenon has been observed in certain frequency ranges that depend on the fiber arrangement and the fiber spacing. Examination of the energy flow associated to the wave motion in the composite has shown that the motion within the stop bands are of a standing-wave type, for which the energy flow is null or very low. For the random fiber arrangement, no clear stop bands have been identified, although significant reduction of the energy transmission has been observed as the frequency increases.

For both periodic and random cases, the computed phase velocities are in good agreement with the theoretical curve given by an existing multiple scattering theory in the long wavelength region, reflecting the insensitivity of the propagation behavior to the detailed microstructure. In the periodic cases, the phase velocity has shown significant variation with the frequency in the vicinity of the stop bands. In the random case, the phase velocity has shown only weak fluctuation from the theoretical curve due probably to the scattering effect by the irregular fiber distribution.

The present analysis has shown the significant influence of the fiber arrangement on the wave propagation behavior in periodic as well as random composites as the wavelength becomes comparable to the fiber spacing. It is the subject of our on-going study to further carry out detailed examination of the influence of the perturbed or random fiber arrangement on the wave propagation characteristics based on the computational procedure described here.

References

Beltzer, A.I., Brauner, N., 1987. The dynamic response of random composites by a causal differential method. Mechanics of Materials 6, 337–345.

Biwa, S., Shibata, T., 2000. Elastic and ultrasonic properties of a unidirectional composite with partially debonded fibres: numerical analysis for longitudinal shear modes. Composites Science and Technology 60, 83–93.

Biwa, S., Watanabe, Y., Ohno, N., 2003. Analysis of wave attenuation in unidirectional viscoelastic composites by a differential scheme. Composites Science and Technology 63, 237–247.

Bose, S.K., Mal, A.K., 1973. Longitudinal shear waves in a fiber-reinforced composite. International Journal of Solids and Structures 9, 1075–1085.

Bose, S.K., Mal, A.K., 1974. Elastic waves in a fiber-reinforced composite. Journal of the Mechanics and Physics of Solids 22, 217–229.

Cai, L.-W., Williams Jr., J.H., 1999a. Large-scale multiple scattering problems. Ultrasonics 37, 453–462.

Cai, L.-W., Williams Jr., J.H., 1999b. Full-scale simulations of elastic wave scattering in fiber-reinforced composites. Ultrasonics 37, 463–482.

Cai, L.-W., Williams Jr., J.H., 1999c. NDE via stop band formation in fiber reinforced composites having square fiber arrangements. Ultrasonics 37, 483–492.

Datta, S.K., Ledbetter, H.M., Kriz, R.D., 1984. Calculated elastic constants of composites containing anisotropic fibers. International Journal of Solids and Structures 20, 429–438.

Feder, J., 1980. Random sequential adsorption. Journal of Theoretical Biology 87, 237–254.

Foldy, L.L., 1945. The multiple scattering of waves. Physical Review 67, 107–119.

Henderson, B.K., Maslov, K.I., Kinra, V.K., 2001. Experimental investigation of acoustic band structures in tetragonal periodic particulate composite structures. Journal of the Mechanics and Physics of Solids 49, 2369–2383.

Huang, W., Rokhlin, S.I., 1995. Frequency dependences of ultrasonic wave velocity and attenuation in fiber composites: theory and experiments. In: Review of Progress in Quantitative Nondestructive Evaluation, vol. 14. Plenum Press, pp. 1233–1240.

Kim, J.-Y., 2003. Antiplane shear wave propagation in fiber-reinforced composites. Journal of the Acoustical Society of America 113, 2442–2445.

Kinra, V.K., Ker, E.L., 1983. An experimental investigation of pass bands and stop bands in two periodic particulate composites. International Journal of Solids and Structures 19, 393–410.

Kittel, C., 1976. Introduction to Solid State Physics, fifth ed. John Wiley & Sons, New York.
Kline, R.A., 1992. Nondestructive Characterization of Composite Media. Technomic Pub, Lancaster.
Kushwaha, M.S., Halevi, P., Dobrzynski, L., Djafari-Rouhani, B., 1993. Acoustic band structure of periodic elastic composites. Physical Review Letters 71, 2022–2025.
Kushwaha, M.S., Halevi, P., Martínez, G., Dobrzynski, L., Djafari-Rouhani, B., 1994. Theory of acoustic band structure of periodic elastic composites. Physical Review B 49, 2313–2322.
Liu, W., Kriz, R.D., 1998. Multiple wave scattering in fiber-reinforced composites: micromechanical viewpoint. Wave Motion 27, 223–244.
Murakami, H., Hegemier, G.A., 1986. A mixture model for unidirectionally fiber-reinforced composites. Transactions of the ASME Journal of Applied Mechanics 53, 765–773.
Naciri, T., Navi, P., Ehrlacher, A., 1994. Harmonic wave propagation in viscoelastic heterogeneous materials: Part I. Dispersion and damping relations. Mechanics of Materials 18, 313–333.
Nelson, R.B., Navi, P., 1975. Harmonic wave propagation in composite materials. Journal of the Acoustical Society of America 57, 773–781.
Pao, Y.-H., Mow, C.-C., 1971. Diffraction of Elastic Waves and Dynamic Stress Concentrations. Crane Russak, New York.
Rokhlin, S.I., Huang, W., Chu, Y.C., 1995. Ultrasonic scattering and velocity methods for characterization of fibre-matrix interphases. Ultrasonics 33, 351–364.
Sobczyk, K., 1985. Stochastic Wave Propagation. Elsevier, Amsterdam.
Talbot, D.R.S., Willis, J.R., 1983. Variational estimates for dispersion and attenuation of waves in random composites: III. Fibre-reinforced materials. International Journal of Solids and Structures 19, 793–811.
Tourin, A., Fink, M., Derode, A., 2000. Multiple scattering of sound. Waves in Random Media 10, R31–R60.
Varadan, V.K., Varadan, V.V., Pao, Y.-H., 1978. Multiple scattering of elastic waves by cylinders of arbitrary cross section: I. SH waves. Journal of the Acoustical Society of America 63, 1310–1319.
Varadan, V.K., Ma, Y., Varadan, V.V., 1986. Multiple scattering of compressional and shear waves by fiber-reinforced composite materials. Journal of the Acoustical Society of America 80, 333–339.
Varadan, V.K., Ma, Y., Varadan, V.V., 1989. Scattering and attenuation of elastic waves in random media. In: Scattering and Attenuation of Seismic Waves, Part II. Birkhauser, Basel, pp. 577–603.
Waterman, P.C., 1969. New formulation of acoustic scattering. Journal of the Acoustical Society of America 45, 1417–1429.
Waterman, P.C., Truell, R., 1961. Multiple scattering of waves. Journal of Mathematical Physics 2, 512–537.
Yang, R.-B., Mal, A.K., 1994. Multiple scattering of elastic waves in a fiber-reinforced composite. Journal of the Mechanics and Physics of Solids 42 (12), 1945–1968.